Effect of seismic source bandwidth on reflection sections to image water structure

R. W. Hobbs,[1] D. Klaeschen,[2] V. Sallarès,[3] E. Vsemirnova,[1] and C. Papenberg[2]

Received 23 July 2009; revised 4 September 2009; accepted 17 September 2009; published 5 November 2009.

[1] The seismic reflection profile is the convolution of the seismic acquisition impulse response and the target impedance contrasts. In the ocean, these contrasts are mainly determined by the widths and gradients of the temperature transitions between the different water masses. Hence seismic oceanography profiles are sensitive to the frequency bandwidth of the seismic acquisition system. We tested a novel seismic source that allowed us to simultaneously profile the ocean with differing impulse responses. We show that frequencies ~20 Hz are best to delineate large impedance contrasts that occur over a vertical scale of several tens of meters whereas frequencies ~80 Hz image the boundaries of layers of around 10 m. We demonstrate a towed acquisition system that can operate from a research vessel to give a bandwidth from 10 to 120 Hz that could, if required, be modified to provide frequencies up to 200 Hz. **Citation:** Hobbs, R. W., D. Klaeschen, V. Sallarès, E. Vsemirnova, and C. Papenberg (2009), Effect of seismic source bandwidth on reflection sections to image water structure, *Geophys. Res. Lett.*, *36*, L00D08, doi:10.1029/2009GL040215.

1. Introduction

[2] Multi-Channel Seismic surveying, a tool used by the hydrocarbons industry to map the subsurface of the Earth, is an excellent tool to study the meso-scale structure of the oceans [*Gonella and Michon*, 1988; *Holbrook et al.*, 2003]. Subsequent research shows that the acoustic reflectivity imaged in the water layer is a direct consequence of the thermohaline structure [*Nandi et al.*, 2004] and the perturbations on the reflective boundaries can be related to the Garrett-Munk internal wave and turbulence spectra [*Holbrook and Fer*, 2005]. Seismic images of water mass fronts and currents [e.g., *Tsuji et al.*, 2005], meso-scale features such as Meddies [*Biescas et al.*, 2008] and the Mediterranean Undercurrent [*Buffett et al.*, 2009] have been recently published, showing the potential of the technique in oceanography. Also by using the UNESCO equations of state for sea-water [*Fofonoff and Millard*, 1983] it is possible to invert the seismic reflectivity to give the physical properties of the sea-water [*Páramo and Holbrook*, 2005].

[3] *Ruddick et al.* [2009] presented a simple means to assess the reflectivity potential of water from conductivity/temperature/depth (CTD) casts by computing the gradient of the impedance (sound speed × density) which approximates to a seismologist's definition of reflectivity. Typically reflection boundaries in the solid Earth have no thickness, i.e., one rock type is juxtaposed to the next with no transition zone, and the reflectivity is assumed to have a "white" spectrum. At low frequencies information is lost because of constructive and destructive interference from fine layers, but as the source bandwidth is shifted to higher frequencies it is possible to resolve ever finer vertical structure (based on the Rayleigh criterion that the vertical resolution limit is one quarter the dominant wavelength) without losing information on the larger scale structure. This is not true for water masses as both heat and mass diffusion produce a gradual change over a finite boundary width that may extend for several tens of meters. Hence in water, the width and the gradient of the boundary makes the reflectivity frequency dependent. There is a similar response for low frequencies as for the solid Earth and as the bandwidth shifts to higher frequencies the vertical resolution increases but this is combined with a loss of information about thicker boundaries with a vertical width of over a seismic wavelength.

[4] The impulse response of the seismic recording system is complex and is influenced by mechanical, geometrical and electrical inputs: the number, size and type of the airguns, the air compressor capacity, the geometry of the source array, and its depth of tow [*Dragoset*, 1990]; the depth of tow of the hydrophone streamer; the directivity response of the receivers; and the filtering both before and after analogue to digital conversion in the seismic data logger. These parameters need to be optimized by detailed modeling prior to the survey to suit the specifications of the vessel [e.g., *Laws et al.*, 1990]. A dedicated vessel will be able to tow source arrays with more than 40 individual airguns and multiple streamers each over 4 km in length. A typical academic research vessel requires a portable system that can be installed specially for the survey. In this case the system is limited, less than 12 airguns and a single streamer of 2.4 km length or at most two short streamers of less than 1 km length.

[5] *Nakamura et al.* [2006] tested different airgun sources to map the boundary between the Kuroshio and the Oyashio water masses. During the GO-project we also tested different air-gun sources: a high-frequency 6-gun mini-GI array; a low-frequency 6-gun Bolt array; and a multi-frequency source with 2 arrays each with 3 Bolt airguns. In this paper we present seismic images from the multi-frequency source. The motivation can be appreciated in Figure 1. Here we show synthetic seismograms for the same input vertical water structure over different bandwidths. If we zoom in onto a part of the XBT cast (see Figure 3 for location) and compare the lower- and higher-frequency responses, it is apparent

[1] Earth Sciences Department, Durham University, Durham, UK.
[2] Leibniz Institute of Marine Geoscience at Kiel University (IFM-GEOMAR), Kiel, Germany.
[3] Unidad de Tecnología Marina, CSIC, Barcelona, Spain.

0094-8276/09/2009GL040215$05.00

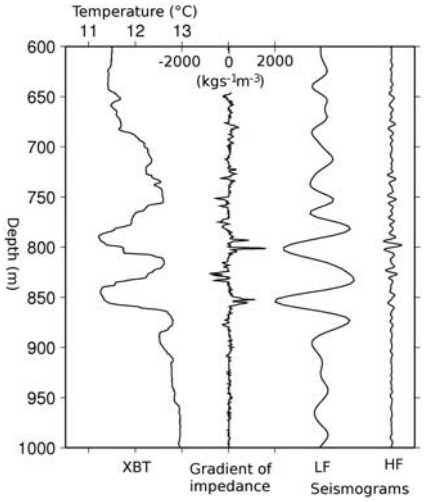

Figure 1. Part of a temperature record from an expendable bathy-thermograph (XBT) through the top reflections close to the centre of the Meddy (location shown in Figure 3), with the vertical derivative of the impedance and two seismograms, computed by deriving the sound speed and density from the XBT data using temperature/salinity/depth relationships [*Käse et al.*, 1996] and forward modeling using finite difference code on the right. The lower frequency (LF) seismogram has a central frequency of 20 Hz whereas the higher frequency (HF) seismogram has a central frequency of 80 Hz.

that the lower-frequency seismogram responds to the large scale features whereas the higher-frequency seismogram is only responding to the smaller scale changes. The challenge was to devise a means to repeat this synthetic experiment during a seismic survey to image water structure given a limited supply of compressed air and tow configurations for the seismic source arrays. The water target is dynamic, so re-shooting a profile with different sources leaves the issue of whether the nature of the boundaries have changed between the two passes. Hence the creation of the multi-resolution (MR) source that provides simultaneous seismic sections of the same water masses so avoiding the issues of acquiring the data at different times.

2. Multi-frequency Source

[6] The source consisted of two separate gun-arrays with 3 air-guns in each array (Figure 2). The lower-frequency (LF) array used 700, 300 and 160 cu in chambers to provide a source rich in low frequency energy and was towed at a nominal depth of 12 m. This gives a source wavelet with a frequency response between 8 and 55 Hz. The upper and lower limit on the bandwidth is determined by notches in the amplitude spectrum caused by destructive interference between the down-going energy and energy reflected at the sea-surface at the source and similarly for the up-going energy at the receiver. The position of these notches are defined by $f_{notch} = nV_{water}/2d$ where V_{water} is the sound-speed of the water, d is the depth of tow of the source or streamer and n=0,1,2. . . , as shown in Figure 2. The higher-frequency (HF) array used 300, 160 and 80 cu in chambers and was towed at a nominal depth of 5.5 m. The frequency response of this array was 12 to 120 Hz. The 2.4 km long hydrophone streamer, with receivers spaced every 12.5 m along its length, was towed at a depth of 5 m. This tow depth is ideal for the HF array as this gives a peak response around 75 Hz, and though the response from the LF array was attenuated the data could still be recovered because of the strong low-frequency signal generated by the inclusion of a 700 cu in gun. By using a second source array tuned to give a better low frequency response we were able to acquire data down to 8 Hz and with improved signal-to-noise (Figure 2b), the amplitude spectrum of the HF array is more than 6 dB lower than the LF array for frequencies below 30 Hz. The two sources were fired alternately, so the odd numbered shots recorded the LF array and the even numbered shots record recorded the HF array. After separating the two datasets and pre-processing to suppress the direct arrival, the data were binned into common mid-point (CMP) gathers; these are groups of seismic traces that have the same geometric mid-point between the source and receiver. Then they are processed in parallel streams that included: source deconvolution (estimated from the sea-floor reflection); muting the upper parts of the longer offset traces to minimize effects of receiver an source directivity; and final bandpass filters set to minimize the bandwidth overlap. During processing care was taken to ensure both sections used the same sound-speed model for the normal move-out correction which is derived from the coincident XBT data using the method devised by *Käse et al.* [1996] based on temperature/salinity/depth calibration from CTD casts performed during the survey.

3. Results

[7] We examine one the profiles acquired during the GO-project cruise, GO-MR-03. This profile was acquired with the MR source described above and crosses a Meddy: an anti-cyclonically rotating eddy of Mediterranean Outflow Water (MOW) that forms from the interaction of the warm saline water flowing out of the Straits of Gibraltar and the Portimao canyon on the southern margin of Iberia. The canyon distrupts the flow and creates Meddies which detach from the main MOW vein on the continental slope at the depth of neutral buoyancy (between 600–1400 m) and drift out into the Gulf of Cadiz and Atlantic Ocean [*Ambar et al.*, 2008]. Figure 3a shows the LF image after filtering to give a processed wavelet with a bandwidth of 10–40 Hz (wavelet and spectrum Figures 3c and 3d); Figure 3b shows the HF image after filtering to give a bandwidth of 40–120 Hz (wavelet and spectrum Figures 3c and 3d). There is an immediate appreciation of the different information content. The LF image best delineates the boundary of a Meddy, whereas the HF image shows more complexity in the reflectivity which makes it more difficult to visualise the water masses. The boxes are shown in Figure 4 to highlight specific differences in the images that illustrate the points made above on the frequency dependence of the reflectivity.

[8] Figure 4a, the LF image from Box 1 (Figure 3), shows part of the lower boundary of the Meddy with a pronounced dipping event. However, in the HF image (Figure 4b) there is no evidence for reflectivity in this region. Our explanation is that there is a gradient change in the temperature profile which is reflective around 20 Hz but is too broad to

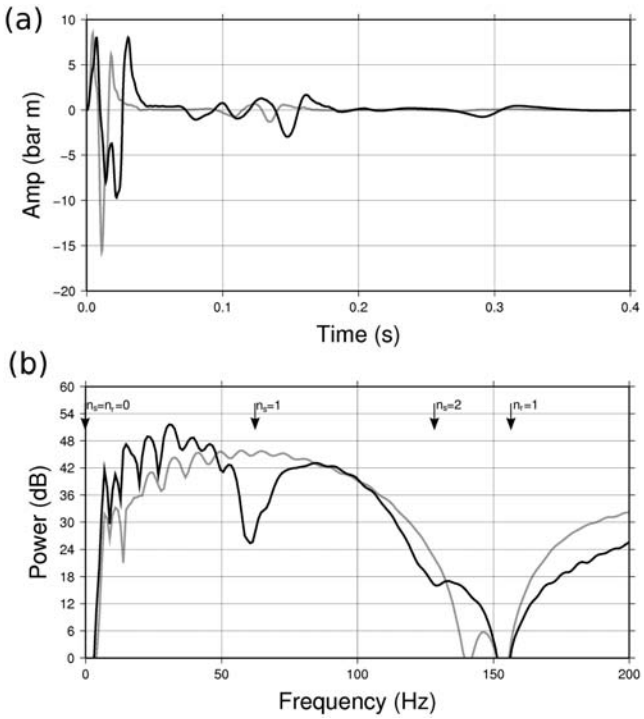

Figure 2. (a) The acquisition wavelet for the LF source (black) and the HF source (gray). The wavelet includes the airgun source; source and receiver free-surface reflections at normal incidence; and instrument filters. The coda following the initial pulse of acoustic energy is caused by reverberations of the residual air-bubble created on firing the airguns with each different airgun volume having its own period. (b) Corresponding amplitude spectra. The free-surface reflection causes notches in the spectra. The location of the source and receiver notches for the LF array are labeled n_s and n_r, respectively.

be reflective at 40 Hz or above is confirmed by examination of the XBT close to CMP 2400. Here a broad temperature perturbation at 1200 m depth can be correlated to a reflection on the LF image but only produces diffuse reflectivity in the HF image. Using 40 Hz as a threshold above which the boundary is no longer reflective gives a minimum thickness of the gradient zone of 38 m, also the maximum thickness is less than about 150 m or it would not be visible on the LF image either. Box 2 from Figure 3 focuses on the base of the Meddy approximately at its center. There is evidence of reflectivity on both sections (Figures 4d and 4e) but the HF image has captured much more detail of the small temperature steps between 1450 and 1600 m depth seen on the XBT cast (Figure 4f). These temperature steps are also seen in the salinity measurements from nearby CTD casts through the base of the Meddy and are the produced by double-diffusion processes involving temperature and salinity [*Hebert*, 1988]. The detail of the steps is lost in the LF image and instead a low amplitude interference pattern is observed that cannot be related to any specific boundary. The final example (Figures 4g and 4h) shows part of the upper boundary of the Meddy. On the LF image there is a second example of an apparent dipping event which when compared with the HF image corresponds to a zone of more complex with sub-horizontal reflections mixed with short dipping events. The coincident XBT (Figure 4i) shows that this location the LF image is highlighting the broader change to higher temperatures at a depth of 900–940 m, whereas the HF image is sensitive to the smaller scale steps on this curve. This example is a combination of the two effects (Boxes 1 and 2) demonstrated above. The LF image is highlighting a broader underlying gradient

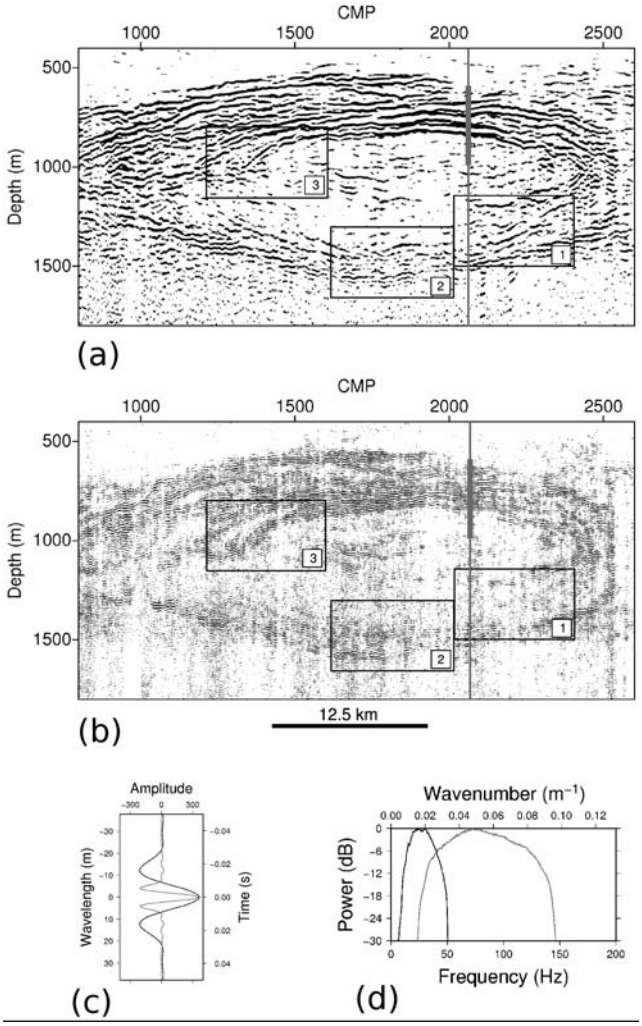

Figure 3. (a) The LF seismic image from profile GO-MR-03 acquired with the lower-frequency source with a processed bandwidth of 10–40 Hz. The reflectivity delineates the shape of the mixed warm-water Meddy lens surrounded by a reflective layer. (b) The HF seismic image from the same profile acquired with the higher-frequency source with a processed bandwidth of 40–120 Hz. The shape of the Meddy is still apparent but the reflectivity appears more diffuse. (c) The effective zero-phase wavelets after processing, LF image, black line and HF image, gray line. (d) Corresponding frequency spectra. The numbered boxes are referred to in the text and are reproduced in Figure 4; and the gray line marks the location of the XBT profile with the thickened line corresponding to the section shown in Figure 1.

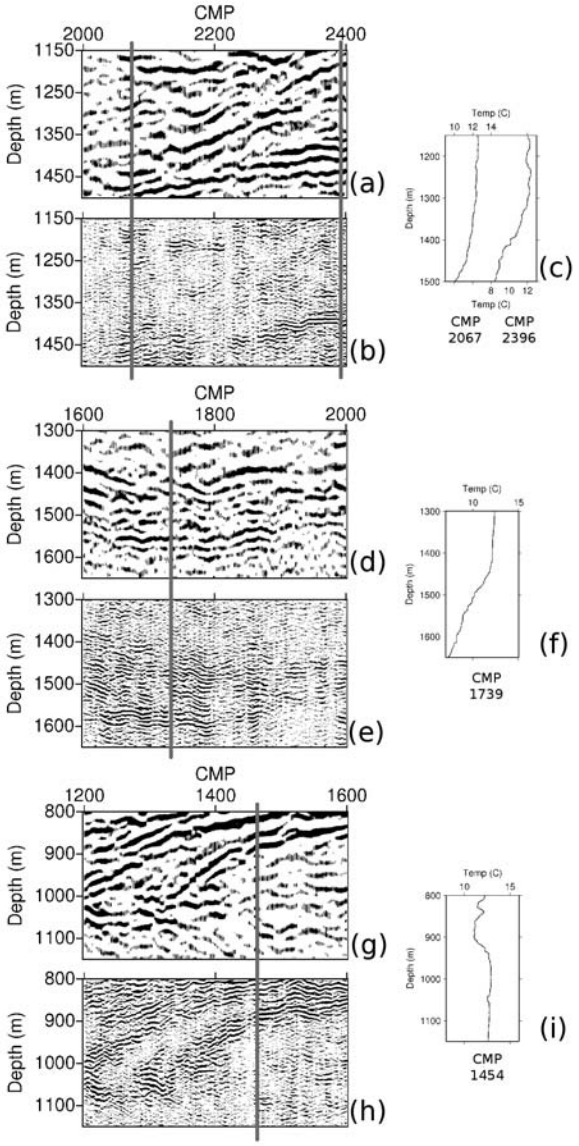

Figure 4. Corresponding (a) LF and (b) HF images for Box 1 (Figure 3) which show an apparent dipping reflector on the LF image that is not reflective on the HF image. (c) Shows intersecting XBT temperature profiles with locations shown as gray lines on seismic sections. (d) LF and (e) HF images for Box 2; here the LF images shows mainly weak reflectivity but the HF image shows complex high amplitude sub-horizontal reflectivity. (f) Shows the intersecting XBT temperature profile. (g) LF and (h) HF images for Box 3; this is a combination of effects shown in Boxes 1 and 2, the LF image shows a single dipping event but the HF image shows a complex zone of horizontal and dipping reflectivity. (i) Shows the intersecting XBT temperature profile.

combined with a interference pattern of the finer-scale structures.

4. Future Design

[9] Though in this profile we only achieved frequencies to 120 Hz, we recommend future systems should try to extend the bandwidth to 200 Hz (vertical resolution of about 2 m) which will capture >95% of the thermohaline acoustic reflectivity. Though there is thermohaline structure on vertical scales of less than 2 m, the associated impedance gradients are too small to image using the seismic method. For conventional large seismic source arrays with a large number of individual air-guns, e.g., the 40-gun 6600 cu in source on the dedicated R/V Marcus Langseth seismic vessel, the source spectrum may be very broad with recoverable energy from less than 10 Hz to above the notches. However, using this extended frequency range is problematical as some processing filters, such as deconvolution, and waveform inversion methods [e.g., *Wood et al.*, 2008]. The lack of energy in the notches means the reflectivity response is unconstrained at these frequencies. To avoid this notch problem and acquire data with a continuous broadband response to 200 Hz means that we have to tow the source and receiver at < 3 m. This is turn limits the low frequency sensitivity, especially for the receiver array, which suppresses the imaging of important lower gradient boundaries in the water layer. Further, to extend the options for seismic oceanography to general research vessels means restricting the number of guns and total compressed air requirement to 'light weight' systems that are portable.

[10] In this paper we have presented a successful two source array solution. To extend the upper frequency limit we recommend target tow depths of 3 and 6 m to give an upper limit of 200 and 100 Hz respectively. The deeper source needs to include at least one large chamber gun, 500 cu in or greater, to provide a strong recoverable low-frequency content. Ideally the arrays should consist of more than 3 guns to give better flexibility to optimize the source wavelet shape by using a larger variety of chamber sizes, and increases acoustic output as the array becomes less efficient as the tow depth is reduced. For an increased bandwidth we suggest a 3-array source with tow depths of 2, 4 and 8 m. Again the same design criteria exist as for the 2-array source with the 8 m depth array will helping ensure a good low-frequency response. A problem with the 3-array solution is that only one in three shots will contribute to each frequency band in the final seismic sections. As successful imaging of water structure relies on summing the seismic traces in the CMP gather to improve the signal to noise ratio, the consequential reduction of the number of traces in each CMP will limit the ability to recover the weaker reflections. Further, if the source impulse responses could be accurately determined on a shot-by-shot basis then, with appropriate phase correction, it should be possible to combine the images, though this presents some major technical challenges.

[11] To directly record the highest frequencies without incurring notches in the frequency response from the free-surface reflection above the hydrophone streamer requires a tow depth of <3 m. This creates a serious issue for physically controlling the array. Its depth is controlled by small paravanes distributed along its length every 100–200 m. These are programmed to maintain the streamer at a set hydrostatic pressure and are strongly damped so they keep the streamer as horizontal as possible., though typically they may deviate by up to 1 m over the length of the streamer. A target tow depth of <3 m requires the surface swell to be <1 m or there is a risk the streamer will breach the surface and all data will be lost. Further, as the swell increases the water

motion creates small intense eddies in the upper 5–6 m of the ocean. If part of the hydrophone streamer passes through one of these eddies, the noise level of the receiver nearest the eddy will increase by several orders of magnitude (swell-breakout) rendering the data useless. To avoid these problems the streamer is towed as deep as possible but this moves the high frequency energy to beyond the receiver notch. Our recommended solution is to use two streamers in an over/under configuration [*Singh et al.*, 1996]. Using this design, the two streamers are towed one above the other at 6 and 9 m to minimizing the risk of breaching and swell-breakout noise. The higher frequency response is recovered by computing the difference in the wavefields recorded on each of the streamers to create a virtual streamer at 3 m. The actual depths will be dictated by operating conditions and the length of the receiver array, the longer the array the greater the minimum separation to avoid entanglement.

5. Conclusions

[12] The results obtained from the GO-MR experiment demonstrates that a single seismic image with a limited bandwidth only provides partial information about the water structure because, unlike the solid Earth, the boundaries between the different water masses are diffuse and therefore their reflectivity is frequency dependent. However, this limitation can be overcome by using a more sophisticated acquisition strategy to provide a broader range of frequencies. We note that the seismic images lacking high frequency content contain apparent isopycnal crossing seismic reflection events that may mislead the interpretation. We believe that these events, observed on our lower-frequency images, are resolved into short isopycnal conformable events when imaged using higher seismic frequencies of 120 Hz (and this will be more evident as frequencies extend towards 200 Hz). This belief is underpinned by the theory of ocean stratification with horizontal mixing being many orders of magnitude greater than vertical mixing. So to obtain maximum information from seismic oceanography requires the collection of broadband seismic data. Design of such a portable 'lightweight' system is a challenge. However we have shown that good results can be obtained by using a dual source and single streamer system. We then propose a more sophisticated approach using multiple sources (2 or even 3 arrays) with a dual depth streamer. The advantages are: the sources can be tuned to give best performance at a range of specified depths; the dual streamer can be towed deeper and therefore seismically quieter which enhances the signal to noise ratio; and the higher frequency energy can be recovered by computing a virtual streamer from the difference in wavefields. By combining the results with appropriate scaling and phase correction gives required broadband response [*Singh et al.*, 1996].

[13] **Acknowledgments.** This GO-project was funded by the EU (015603-GO-STREP). RWH was funded as a NERC Advanced Research Fellow (NER/J/S/2002/00745). Seismic data was processed using Landmark Promax (University Partnership) and Seismic Unix Software. The authors thank the officers and crew on the RRS Discovery for their professional assistance during the GO cruise. Also the reviewers whose comments have improved the paper.

References

Ambar, I., et al. (2008), Observations of the Mediterranean undercurrent and eddies in the Gulf of Cadiz during 2001, *J. Mar. Syst.*, *71*, 195–220, doi:10.1016/j.jmarsys.2007.07.003.

Biescas, B., V. Sallarès, J. L. Pelegrí, F. Machín, R. Carbonell, G. Buffett, J. J. Dañobeitia, and A. Calahorrano (2008), Imaging meddy finestructure using multichannel seismic reflection data, *Geophys. Res. Lett.*, *35*, L11609, doi:10.1029/2008GL033971.

Buffett, G., B. Biescas, J. L. Pelegrí, F. Machín, V. Sallares, R. Carbonell, D. Klaeschen, and R. Hobbs (2009), Seismic reflection along the path of the Mediterranean undercurrent, *Cont. Shelf Res.*, *29*, 1848–1860, doi:10.1016/j.csr.2009.05.017.

Dragoset, W. H. (1990), Air-gun array specs: A tutorial, *Leading Edge*, *9*, 24–32, doi:10.1190/1.1439671.

Fofonoff, N. P., and R. C. Millard Jr. (1983), Algorithms for computation of fundamental properties of seawater, *Tech. Pap. Mar. Sci. 44*, UNESCO, Paris.

Gonella, J., and D. Michon (1988), Deep internal waves measured by seismic-reflection within the eastern Atlantic water mass (in French with English abstract), *C. R. Acad. Sci., Ser. II*, *306*, 781–787.

Hebert, D. (1988), Estimates of salt finger fluxes, *Deep Sea Res., Part A*, *35*, 1887–1901, doi:10.1016/0198-0149(88)90115-X.

Holbrook, W. S., and I. Fer (2005), Ocean internal wave spectra inferred from seismic reflection transects, *Geophys. Res. Lett.*, *32*, L15604, doi:10.1029/2005GL023733.

Holbrook, W. S., P. Paramo, S. Pearse, and R. W. Schmitt (2003), Thermohaline fine structure in an oceanographic front from seismic reflection profiling, *Science*, *301*, 821–824, doi:10.1126/science.1085116.

Käse, R. H., H. H. Hinrichsen, and T. Sanford (1996), Inferring density from temperature via a density-ratio relation, *J. Atmos. Oceanic Technol.*, *13*, 1202–1208, doi:10.1175/1520-0426(1996)013<1202:IDFTVA>2.0.CO;2.

Laws, R. M., L. Hatton, and M. Haartsen (1990), Computer modelling of clustered airguns, *First Break*, *8*, 331–338.

Nakamura, Y., T. Noguchi, T. Tsuji, S. Itoh, H. Niino, and T. Matsuoka (2006), Simultaneous seismic reflection and physical oceanographic observations of oceanic finestructure in the Kuroshio extension front, *Geophys. Res. Lett.*, *33*, L23605, doi:10.1029/2006GL027437.

Nandi, P., W. S. Holbrook, S. Pearse, P. Páramo, and R. W. Schmitt (2004), Seismic reflection imaging of water mass boundaries in the Norwegian Sea, *Geophys. Res. Lett.*, *31*, L23311, doi:10.1029/2004GL021325.

Páramo, P., and W. S. Holbrook (2005), Temperature contrasts in the water column inferred from amplitude-versus-offset analysis of acoustic reflections, *Geophys. Res. Lett.*, *32*, L24611, doi:10.1029/2005GL024533.

Ruddick, B., H. Song, C. Dong, and L. Pinheiro (2009), Water column seismic images as maps of temperature gradient, *Oceanography*, *22*, 193–205.

Singh, S. C., R. W. Hobbs, and D. B. Snyder (1996), Broad-band receiver response from dual-streamer data and applications in deep reflection seismics, *Geophysics*, *61*, 232–243, doi:10.1190/1.1443944.

Tsuji, T., T. Noguchi, H. Niino, T. Matsuoka, Y. Nakamura, H. Tokuyama, S. Kuramoto, and N. Bangs (2005), Two-dimensional mapping of fine structures in the Kuroshio current using seismic reflection data, *Geophys. Res. Lett.*, *32*, L14609, doi:10.1029/2005GL023095.

Wood, W. T., W. S. Holbrook, M. K. Sen, and P. L. Stoffa (2008), Full waveform inversion of reflection seismic data for ocean temperature profiles, *Geophys. Res. Lett.*, *35*, L04608, doi:10.1029/2007GL032359.

R. W. Hobbs and E. Vsemirnova, Earth Sciences Department, Durham University, South Road, Durham DH1 3LE, UK. (r.w.hobbs@durham.ac.uk)

D. Klaeschen and C. Papenberg, Leibniz Institute of Marine Geoscience at Kiel University (IFM-GEOMAR), D-24148 Kiel, Germany.

V. Sallarès, Unidad de Tecnología Marina, CSIC, Passeig Maritim de la Barceloneta 37-49, E-08003 Barcelona, Spain.